Mechanical properties of ZnS nanowires and thin films: Microscopic origin of the dependence on size and growth direction

Taraknath Mandal,* Prabal K. Maiti,† and Chandan Dasgupta‡
Centre for Condensed Matter Theory, Department of Physics, Indian Institute of Science, Bangalore 560012, India
(Received 23 September 2011; revised manuscript received 19 April 2012; published 9 July 2012)

Mechanical properties of ZnS nanowires and thin films are studied as a function of size and growth direction using all-atom molecular dynamics simulations. Using the stress-strain relationship we extract Young's moduli of nanowires and thin films at room temperature. Our results show that Young's modulus of [0001] nanowires has strong size dependence. On the other hand, [01$\bar{1}$0] nanowires do not exhibit a strong size dependence of Young's modulus in the size range we have investigated. We provide a microscopic understanding of this behavior on the basis of bond stretching and contraction due to the rearrangement of atoms in the surface layers. The ultimate tensile strengths of the nanowires do not show much size dependence. To investigate the mechanical behavior of ZnS in two dimensions, we calculate Young's modulus of thin films under tensile strain along the [0001] direction. Young's modulus of thin films converges to the bulk value more rapidly than that of the [0001] nanowire.

DOI: 10.1103/PhysRevB.86.024101 PACS number(s): 62.20.de, 62.23.Hj, 62.23.Kn, 62.20.mj

I. INTRODUCTION

Designing a nanoscale device requires detailed information about the mechanical properties of materials at the nanoscale. Properties at the nanoscale can be very different from those of bulk systems because of higher surface to volume ratio. Over the last few decades, ZnS has attracted considerable attention due to its potential applications in electroluminescent devices, displays, sensors and lasers.[1,2] ZnS nanostructures are being used in electronics, optoelectronics, and nanodevices.[3–10] In recent years, ZnS nanostructures with various shapes, such as nanowires, nanospheres, nanobelts, nanosheets, and nanotubes have been synthesised.[3,11–20] The most common growth direction for ZnS nanowires and nanobelts is [0001] with the wurtzite structure.[4,7] One-dimensional structures in the [01$\bar{1}$0] direction have also been synthesized.[3] Growth of ZnS thin films has also been reported.[21]

Knowledge of mechanical properties of nanowires is very important for their usage in various nanodevices where mechanical response is used to achieve desired functionality. Various experimental techniques, such as atomic force microscopy (AFM)–based three-point bending technique,[22] transmission electron microscopy (TEM),[23] and nanoindentation,[22,24] have been used to characterize the mechanical properties of various nanowires and thin film systems. In these experimental efforts, mechanical properties of ZnO nanostructures in particular have been investigated extensively. Molecular simulations employing large-scale atomistic molecular dynamics (MD) simulation using two-body pair potentials,[23,25,26] as well as density functional theory (DFT),[27] have also been used to validate some of the experimental results and to give a microscopic picture. In contrast, for ZnS nanowires and thin films, only very limited experimental information is currently available on their mechanical properties. Li *et al.*[28] found that ZnS nanobelts, which are micrometers in length and 50–100 nm in thickness, exhibit a Young's modulus of 35.9 $\pm$ 3.5 GPa. Using force-deflection spectroscopy, they also measured Young's modulus of ZnS nanobelts and found it to be 52 $\pm$ 7.0 GPa.[29] These values are smaller than Young's modulus of bulk wurtzite ZnS. However, using the same method, they measured Young's modulus of ZnO nanobelts, which are 50–140 nm in thickness and 270–700 nm in length, and the measured value was 38.2 $\pm$ 1.8 GPa, which is smaller than the bulk Young's modulus value,[22] whereas other experimental results show that Young's modulus of ZnO nanowires is larger than that of the bulk.[23,30] Recently Chen *et al.*[31] investigated Young's modulus of pristine, as well as hydrogen- and water-absorbed ZnS nanowires using all-electron density functional theory. They found that Young's moduli of the pristine and water-absorbed nanowires are larger, but those of the hydrogen-absorbed nanowires are smaller, than that of bulk ZnS. Although there exist some theoretical frameworks to explain and predict the elastic properties of a variety of nanostructures,[32,33] the size dependence of Young's modulus of ZnS at the nanoscale is still controversial.

To help resolve the above controversy, in the present work, we evaluate Young's moduli and ultimate tensile strengths of ZnS nanowires of sizes ranging from 3 to 7 nm and those of ZnS thin films of thickness ranging from 0.8 to 3 nm by MD simulations. We present here our results for the size and orientation dependence of these mechanical properties. Table I summarizes the details of the system sizes used in this study.

II. METHODOLOGY

All nanowires and thin films used in this study are single crystalline, cut from supercells of wurtzite crystal. Initial configurations of the nanowires and thin films were generated using Cerius2.[34] Figure 1 shows the different geometry of the nanowires and thin films used in this study. Details of the conventions to determine the sizes of nanowires and thin films are given in the supplementary material.[35] The Zn and S atoms have charges of $+2$ and -2, respectively. Interatomic interaction between Zn-Zn, Zn-S, and S-S are described by the Buckingham potential given by

$$U_{ij} = A_{ij} \exp\left(\frac{-R_{ij}}{\rho_{ij}}\right) - \frac{C_{ij}}{R_{ij}^6}, \quad (1)$$

TABLE I. Details of system sizes considered in this study.

Cylindrical nanowires				Faceted nanowires				Thin films	
[0001]		[01$\bar{1}$0]		[0001]		[01$\bar{1}$0]		[0001]	
Diameter (nm)	No. of atoms	Diameter (nm)	No. of atoms	Breadth (nm)	No. of atoms	Breadth (nm)	No. of atoms	Thickness (nm)	No. of atoms
3	4758	2	2140	1.15	2160	1.65	2486	0.8	3776
4	8654	3	5030	1.53	3840	2.30	4474	1.5	6336
5	13208	4	8532	1.91	6000	2.95	7030	2.3	8896
6	18000	5	12520	2.29	8638	3.34	8520	3.0	11456
7	26640	—	—	2.68	11760	—	—	—	—
—	—	—	—	3.06	15360	—	—	—	—

where U_{ij} is the interaction potential, R_{ij} is the distance between atoms i and j, and A_{ij}, ρ_{ij}, and C_{ij} are three model parameters. An angle-bending interaction of the form

$$U_{ijk} = \tfrac{1}{2} K_{ijk}(\theta - \theta_{ijk})^2 \quad (2)$$

is used to describe the three-body interaction for S-Zn-S atoms.

The interaction parameters are taken from Ref. 36. To test the applicability of these parameters in the case of the ZnS nanostructure, we also carried out DFT optimization of the structure of a 0.76-nm faceted [0001] nanowire. The DFT calculation is done within the Perdew-Burke-Ernzerhof (PBE)–corrected generalized gradient approximation (GGA)[37] as implemented in the Quantum Espresso package.[38] The relaxation of the structure is done keeping the nanowire at the middle of a supercell. The dimensions of a and b of the supercell are kept such that the distances between the nanowire and its periodic images are approximately 10 Å. The dimension of the supercell along the c axis is the same as that of the nanowire. The integration over the Brillouin zone is performed over Monkhorst-Pack[39] $2 \times 2 \times 6$ k-point meshes. The electron wave functions are expanded in the plane wave basis set with a cut-off energy of 30 Ry, and plane waves with kinetic energy of up to 300 Ry are used for the charge density. Results of the DFT calculation and a comparison with MD results are shown in Figure 2 and Table II, respectively. Our DFT-optimized faceted ZnS nanowire yields similar lattice constants as those

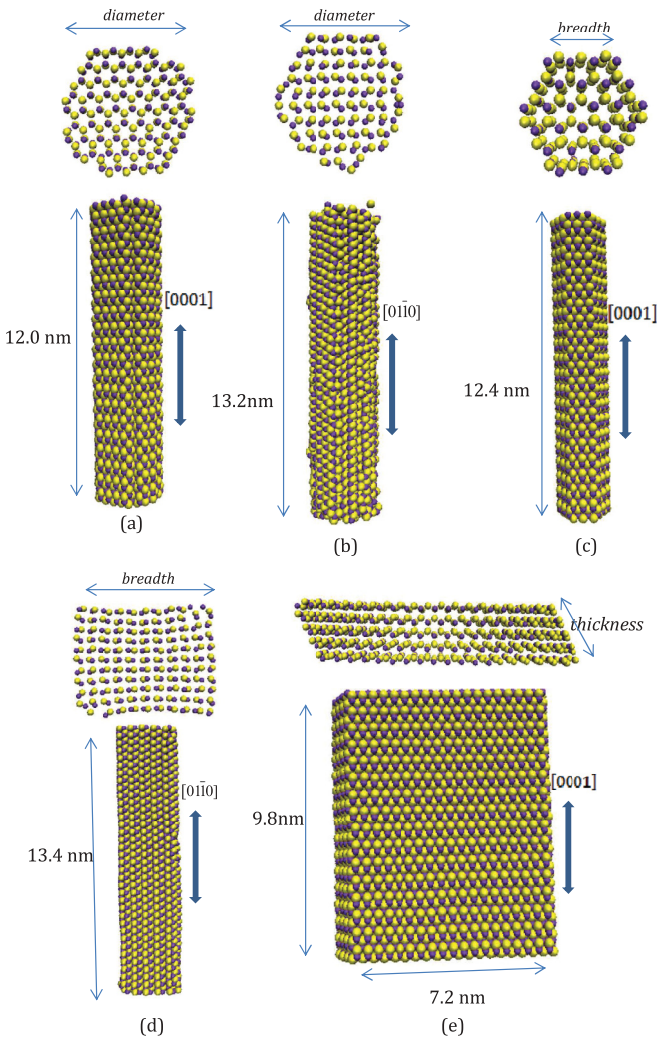

FIG. 1. (Color online) Equilibrated structures of (a) 3-nm [0001] cylindrical nanowire, (b) 3-nm [01$\bar{1}$0] cylindrical nanowire, (c) 1.15-nm [0001] faceted nanowire, (d) 3.34-nm [01$\bar{1}$0] faceted nanowire, and (e) 1.5-nm thin film. At the top, cross-sectional views are shown. Bold arrows indicate the straining direction.

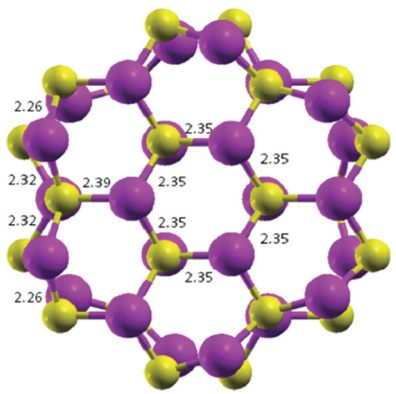

FIG. 2. (Color online) DFT optimized structure of faceted ZnS nanowire containing 48 atoms. Yellow (light gray) atoms are sulfur, and violet (gray) atoms are zinc. The numbers indicate the bond lengths. Movements of atoms (increment and decrement of bond lengths) occur at the two outermost layers only. The core region remains unchanged.

TABLE II. Comparison of lattice constants obtained from density functional theory (DFT) and molecular dynamics (MD) calculations.

	a (Å)	c (Å)
Experimental	3.811,[46] 3.823[47]	6.234,[46] 6.261[47]
Other theoretical results	3.84,[48] 3.777,[49] 3.91,[42] 3.982[50]	6.267,[48] 6.188,[49] 6.05,[42] 6.50[50]
MD results (this work)	3.82	6.26
DFT results (this work)	3.84	6.30

obtained using the above interaction parameters. Also, in recent years, several studies have demonstrated that using a two-body interaction like the Buckingham potential without including any bond stretching, angle bending, dihedral potential can describe the mechanical properties of nanowires very well.[23,25,26] This gives us confidence that the results obtained for the ZnS nanowires and thin films using the above interaction potential will be quite accurate and can work for other similar nanosystems. In all three directions, a periodic boundary condition was enforced using a supercell concept, in which the simulation box is defined to be considerably larger than the diameter of nanowires in two directions or thickness of thin films in one direction. We placed the nanowires in the middle of the simulation box, whose length along the growth direction is the same as that of the nanowire; along the other two directions, box lengths are 15 nm. Thus, the distances between the nanowire and its periodic images are 8 nm for the largest nanowire (7 nm). For the thin films, the dimensions of the simulation box along the x and z directions are the same as those of the thin films, and along the y direction, the box length is 15 nm. The particle-particle mesh Ewald sum was used for calculating the electrostatic interactions. A similar method was used for Ewald sum calculations of long-range coulomb interactions in ZnO nanobelts by Kulkarni *et al.* [25]

The initial configurations generated by Cerius2 were first equilibrated at constant pressure for 70 ps and then at constant volume for another 70 ps at 300 K temperature. To check the effect of initial configurations, we also carried out longer equilibration for 140 ps before subjecting the nanowire to tensile load, and the final results were found to be the same as those in the previous case. The tensile process was carried out by separating a few of the top and bottom layers of atoms, considering them to be two rigid blocks, in a stepwise manner. For each step, the nanowire was stretched by 0.5 Å and equilibrated for 100 ps. A similar protocol was used for thin films as well.

III. RESULTS AND DISCUSSION

Figure 3 shows the stress-strain curves of cylindrical nanowires under applied strain. Nanowires with different growth directions show distinctly different behavior. The [0001] nanowires show elastic response up to a strain of 4–7% followed by a plastic region. On the other hand, the [01$\bar{1}$0] nanowires remain elastic up to a relatively higher strain (∼8–11%) compared with the [0001] nanowires, and they do not have any well-defined plastic region. We also find that none of the nanowires shows strain softening (i.e., a decrease in the stress value with increasing strain). The ultimate tensile strength (UTS) (the maximum of the stress-strain response) and the breaking stress are almost the same, which reflects the brittle nature of the nanowires. We have also shown the stress-strain response for faceted nanowires in Figure 4. The response is qualitatively similar to that of cylindrical nanowires: strong size dependence in the [0001] direction and very weak size dependence in the [01$\bar{1}$0] direction.

Figure 5 shows instantaneous snapshots of the breaking of a 4-nm [01$\bar{1}$0] cylindrical nanowire. As shown in the figure, it breaks suddenly at about 13% strain without formation of amorphous or necking regions. Similar behavior is seen in all other nanowires and thin films. It reflects the fact that they are highly brittle in nature. We do not see any kind of phase transformation, denoted by deformation beyond the elastic regime typically found for some metallic and semiconducting materials,[25,40,41] in either nanowires or thin films.

From the stress-strain curves, we have calculated Young's modulus of ZnS nanowires grown along [0001] and [01$\bar{1}$0] directions. These values are given in Tables III and IV. Note that the calculated Young's modulus for bulk ZnS is in good agreement with available theoretical[31] and experimental results.[42] In Figure 6(a) and 6(b), we have plotted Young's modulus as a function of nanowire size for two different growth directions. Clearly, there is a strong size dependence for the [0001] nanowires. Young's modulus decreases with increasing size. More precisely, Young's modulus increases by as much as

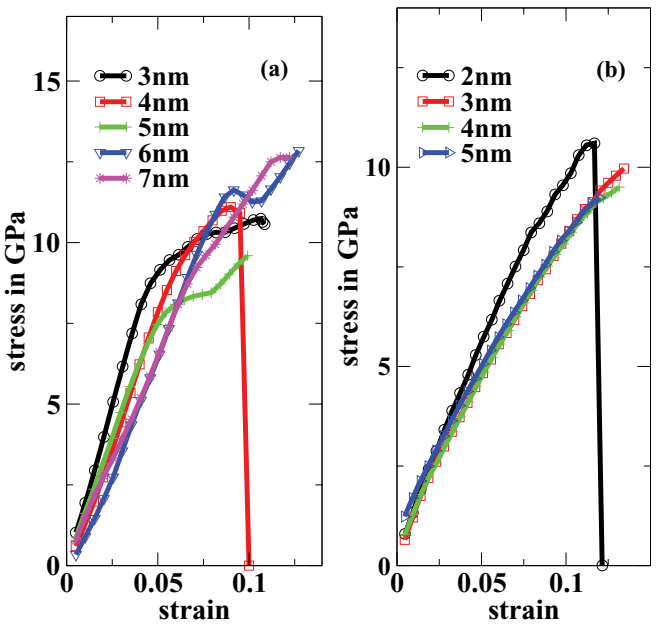

FIG. 3. (Color online) Stress-strain curves for (a) [0001] and (b) [01$\bar{1}$0] cylindrical nanowires during the loading process. Sharp vertical lines show the breaking (shown for only one case for each direction).

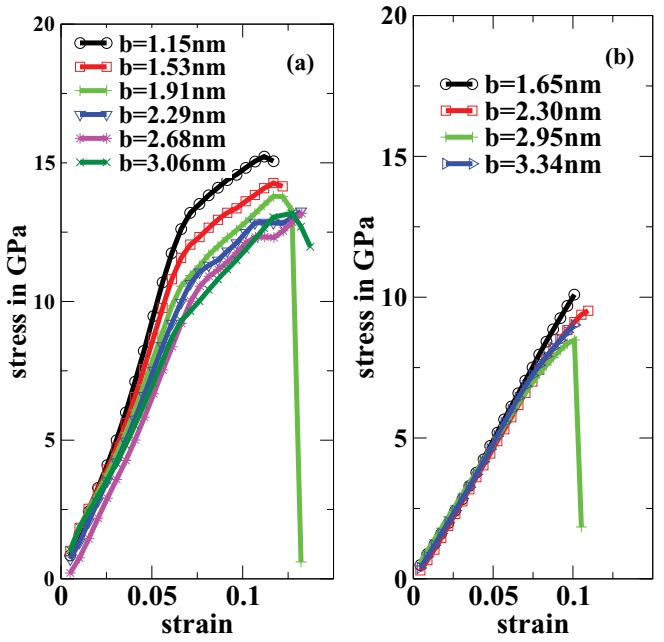

FIG. 4. (Color online) Stress-strain curves for (a) [0001] and (b) [01$\bar{1}$0] faceted nanowires during the loading process. Sharp vertical lines show the breaking (shown only for one case for each direction).

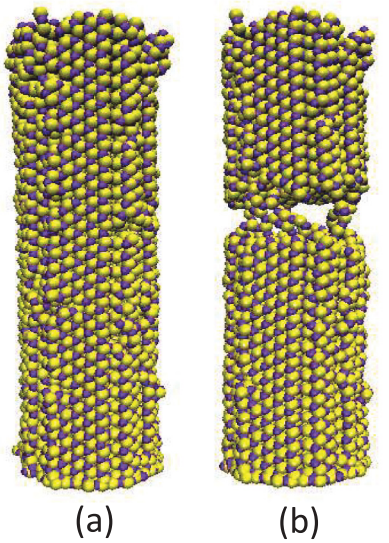

FIG. 5. (Color online) Breaking of a 4-nm [01$\bar{1}$0] cylindrical nanowire. (a) Snapshot of the nanowire just before breaking. (b) Snapshot after braking. The sudden breaking represents the brittleness of the nanowire.

57%, 29%, 21%, and 12% for 3-, 4-, 5-, and 6-nm cylindrical nanowires, respectively, compared with the bulk. On the other hand, the [01$\bar{1}$0] nanowires do not show much size dependence within the simulated size range. Young's modulus of the 2-nm cylindrical nanowire is 18% greater than the bulk value, and 4- and 5-nm nanowires have Young's modulus values very similar to the bulk value. The observed size dependence of Young's modulus can be explained on the basis of induced surface stress produced by the movement of surface atoms, as shown in Figures 7 and 8. In the nanowires, atoms at a free surface experience a different local environment than atoms in the core of the nanowire, which is more bulk-like. As a result, the energies of these surface atoms are different from those of the core atoms. To minimize this excess energy, the surface atoms change their positions, and this surface reconstruction causes a movement of the outer surface layers. Figure 7(a) shows a cross-sectional view of a zero-temperature minimized structure of a 1.53-nm faceted [0001] nanowire. We see that rearrangements of atoms occur in the two outermost layers only. As shown in Figure 7(b) the bond lengths between S and Zn atoms in the third and fourth layers from outside are close to the bulk value of 2.33 Å, indicating no reorganization of atoms

TABLE III. Young's moduli and ultimate tensile strength (UTS) of cylindrical nanowires of various diameters in different growth directions. Young's modulus and UTS of ZnS thin films of various thickness are also given along with Young's modulus of bulk ZnS in different growth directions.

	Young's modulus (GPa)		UTS (GPa)	
Cylindrical nanowires	[0001]	[01$\bar{1}$0]	[0001]	[01$\bar{1}$0]
Diameter (nm)				
2	—	110.2	—	10.60
3	200.9	98.28	10.74	9.97
4	164.4	94.05	11.09	9.50
5	154.5	92.98	9.59	9.24
6	143.6	—	12.84	—
7	127.7	—	12.64	—
Thin films				
Thickness (nm)				
0.8	180.6		15.19	
1.5	157.8		12.86	
2.3	139.0		11.31	
3.0	133.3		12.84	
Bulk	127.9 (118,[42] 128[31])	93.41 (91[42])		

TABLE IV. Young's moduli and ultimate tensile strength (UTS) of faceted nanowires of various breadths in (a) [0001] and (b) [01$\bar{1}$0] directions.

Faceted nanowires	Young's modulus (GPa)	UTS (GPa)
(a) Breadth (nm)	[0001]	
1.15	196.5	15.22
1.53	173.8	14.27
1.91	156.9	13.79
2.29	153.8	12.85
2.68	149.3	13.17
3.06	134.8	13.18
Bulk	127.9 (118,[42] 128[31])	—
(b) Breadth (nm)	[01$\bar{1}$0]	
1.65	102.3	10.09
2.30	96.76	9.51
2.95	92.28	8.48
3.34	98.11	9.02
Bulk	93.41 (91[42])	—

in these layers. Variations of the bond lengths between atoms in the first and second layers and the second and third layers represent the movements of atoms at the outermost two layers. Figure 7(c) shows that the distances between atoms (here the Zn-Zn distance) at the fourth and second layers increase from their bulk value of 3.83 Å. However, distances between atoms at the first and third layers decrease, which confirms that the outermost layer comes inside, and the second outermost layer moves out, as shown by the bold arrows in the figure. The

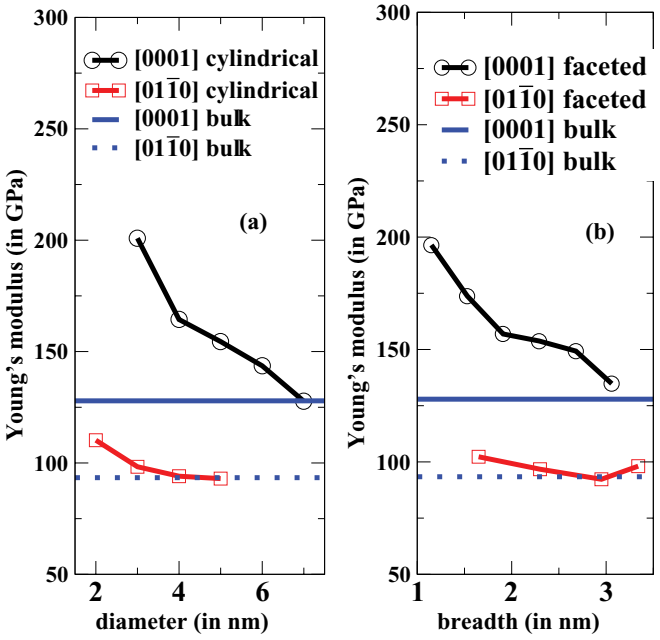

FIG. 6. (Color online) Size dependence of Young's modulus of (a) cylindrical nanowires and (b) faceted nanowires for various growth directions.

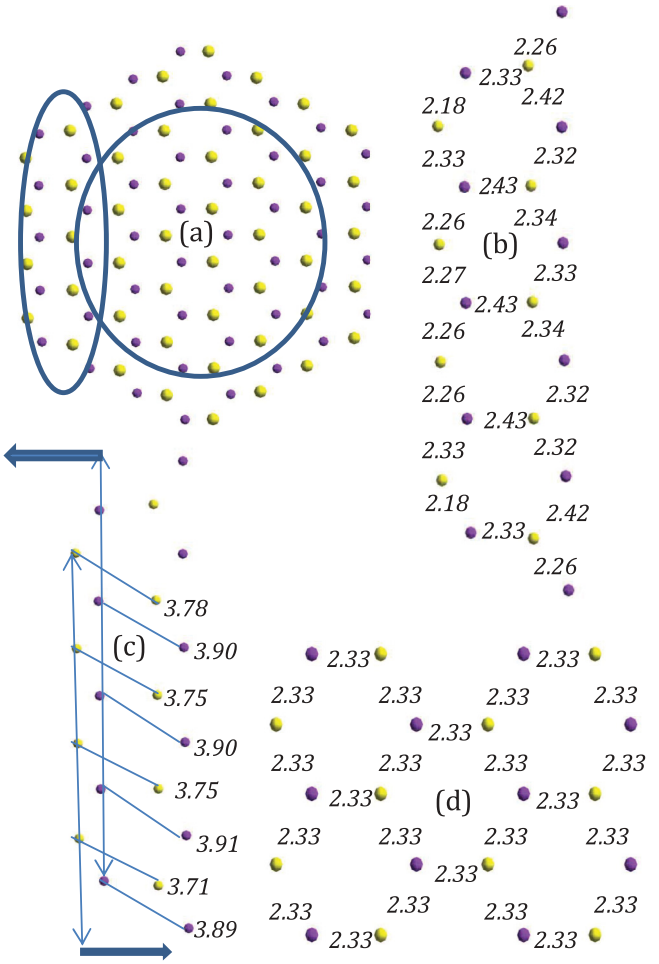

FIG. 7. (Color online) (a) Cross-sectional view of minimized structure (corresponding to zero temperature) of 1.53-nm faceted nanowire. Violet (gray)atoms are zinc, and yellow (light gray) atoms are sulfur. (b) Bond lengths in four outermost layers are shown. Bond lengths between third and fourth layers do not change; movement of atoms occurs at outermost two layers only. (c) Increases and decreases in zinc-zinc and sulfur-sulfur distances indicate that the outermost layer (here, the S layer) comes inside and second outermost layer goes outside. (d) Core region remains unchanged.

inside core region remains unaffected, as shown in Figure 7(d). Similar kinds of surface modification are observed for all other faceted, as well as cylindrical, [0001] nanowires.

In contrast, the [01$\bar{1}$0] nanowires show a very different behavior. In these nanowires, both the surface atoms and atoms at the core regions change their positions. In Figure 8(c), a cross-sectional view of the zero-temperature minimized structure of a 3-nm [01$\bar{1}$0] cylindrical nanowire is shown. Figure 8(d) focuses on the core region, which shows variations of bond lengths. In Figures 8(a) and 8(b), we show cross-sectional views of a 3-nm [0001] cylindrical nanowire to illustrate the contrasting behavior.

To understand this distinct behavior, we plot the average potential energy (PE) per particle in Figure 9(a). The surface to volume ratio increases with decreasing lateral dimension and results in excess surface energy for thinner nanowires. The excess surface energy results in higher average energy values for thinner nanowires. From Figure 9(a), we also find

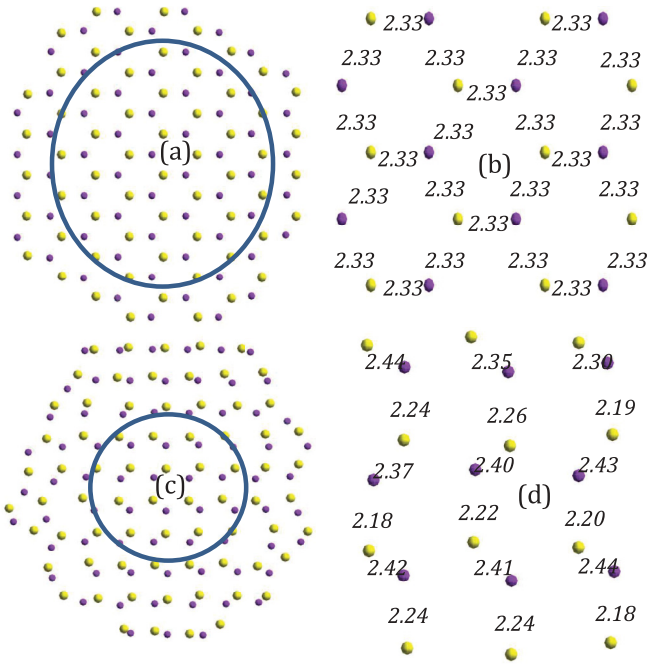

FIG. 8. (Color online) (a) Cross-sectional view of zero-temperature minimized 3-nm [0001] cylindrical nanowire. (b) Bond lengths show that the core region is unaffected. (c) Zero-temperature minimized 3-nm [01$\bar{1}$0] cylindrical nanowire. (d) Variations of the bond lengths indicate that the structure of the core region is modified.

that the average PE per particle for [01$\bar{1}$0] nanowires is higher compared with that for [0001] nanowires. The difference of average energy per particle for two different growth directions

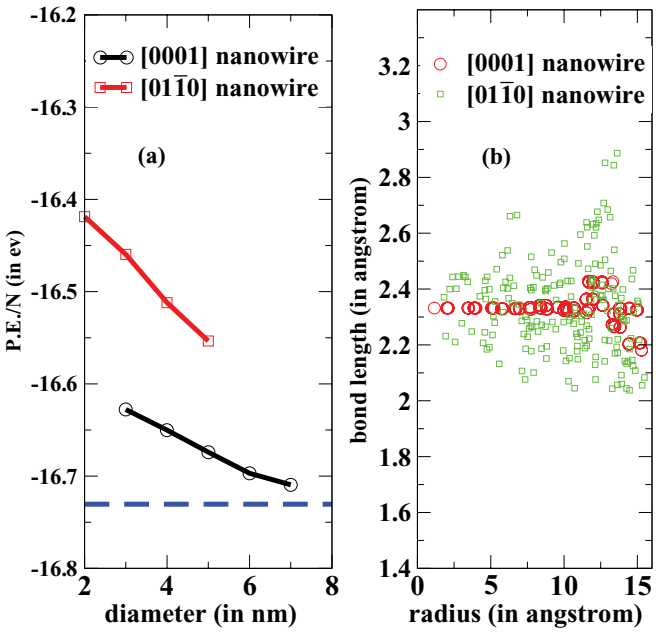

FIG. 9. (Color online) (a) Average potential energy (P.E.) per particle for the cylindrical nanowires. The dotted line corresponds to the potential energy per particle in the bulk material. (b) Bond length distribution of 3-nm [0001] and [01$\bar{1}$0] cylindrical nanowires. In the [0001] nanowire, movement of atoms occurs at the surface only, whereas in the [01$\bar{1}$0] nanowire, core atoms are also displaced.

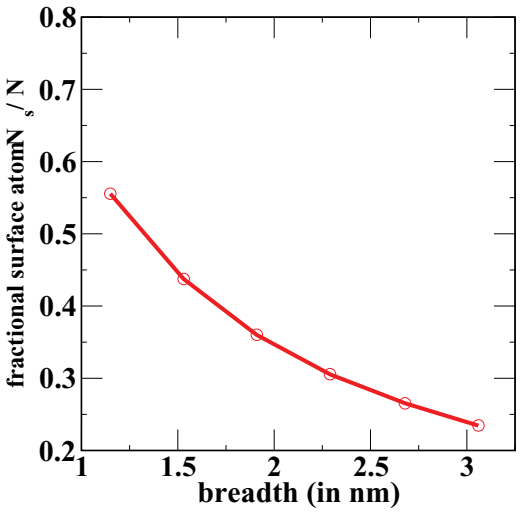

FIG. 10. (Color online) Variation of fractional surface atoms as a function of breadth of [0001] faceted nanowires.

appears because different surfaces of ZnS have different energy. The surface energies of {0001} surfaces of ZnS were shown to be much higher compared with the energies of {01$\bar{1}$0} or {11$\bar{2}$0} surfaces. Surface energies of {01$\bar{1}$0}, {11$\bar{2}$0}, and {0001} surfaces are 0.51, 0.32, and 1.50 J/m^2, respectively.[43] Nanowires grown along the [0001] axis contain relatively lower energetic {01$\bar{1}$0} and {11$\bar{2}$0} surfaces. On the other hand, nanowires grown along the [01$\bar{1}$0] axis have more energetic polar {0001} surfaces and {11$\bar{2}$0} surfaces. More energetic {0001} surfaces of the [01$\bar{1}$0] nanowires cause the surface energy for these nanowires to be higher. The lower average energy per atom for {0001} nanowires indicates this is the most favorable growth direction.[44,45] The high value of surface energy for the [01$\bar{1}$0] nanowires causes the surface atoms to relax spontaneously to a large extent. Because of the large movements of the surface atoms, the positions of the atoms in the core region also get modified to minimize the total energy. To probe the surface reconstruction further, we have calculated the bond length distributions as a function of radius for 3-nm cylindrical nanowires in both directions. As we see in Figure 9(b), bond length fluctuations are much more pronounced in the [01$\bar{1}$0] nanowire and occur in all the layers, leaving no distinction between the surface and core regions. Because there are no well-defined surface or core regions, we calculate the average bond length over the entire structure and find the mean bond length to be the same as that of the bulk. In contrast, for [0001] nanowires, fluctuations in the bond lengths are localized at the surface layers only, and we observe that there is a decrease of ~0.07 Å in the mean bond length at the surface region.

An overall decrease of the mean bond length in the outer layers for the [0001] nanowires increases the average binding energy of the surface atoms. Extra energy is required to stretch these surface atoms because of the higher binding energy, which increases the Young's modulus value. However, the surface atoms to total atoms ratio decreases with size, as shown in Figure 10. In thicker nanowires, the surface effect is negligible; hence, their Young's modulus values converge to the bulk value. The UTSs do not have any size dependence

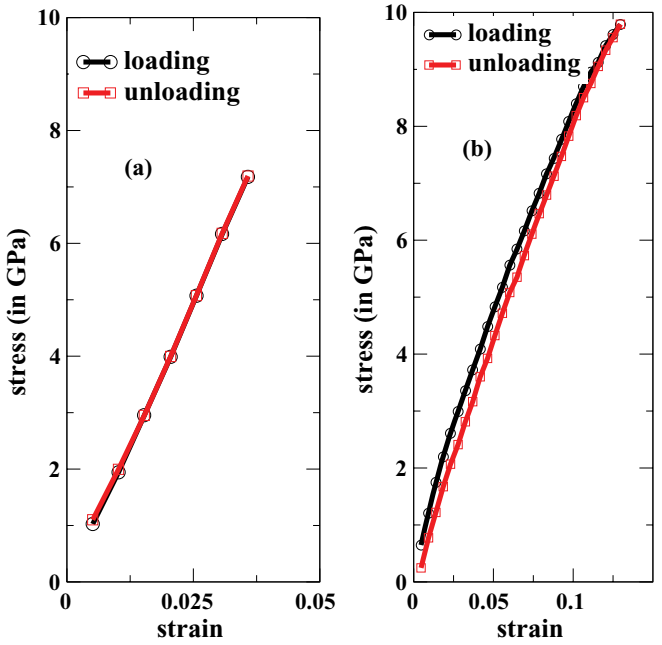

FIG. 11. (Color online) Stress strain curves for (a) 3-nm [0001] and (b) 3-nm [01$\bar{1}$0] cylindrical nanowire during loading and unloading process.

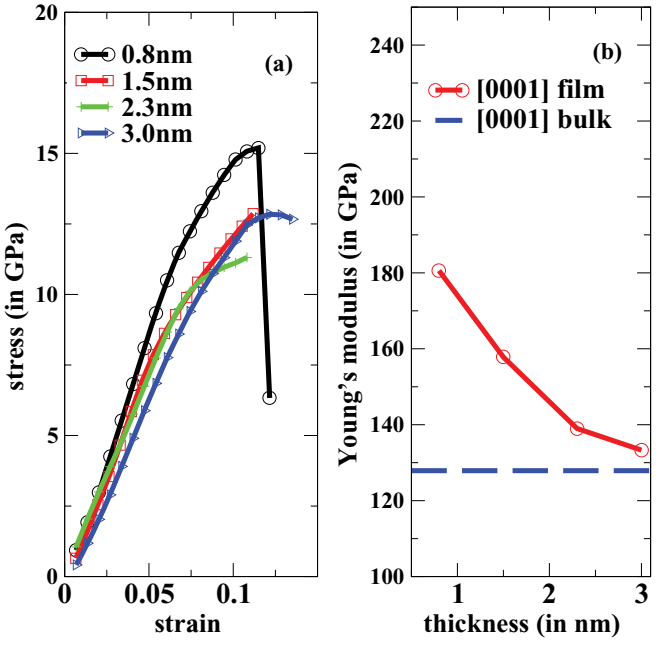

FIG. 12. (Color online) (a) Stress-strain curves for thin films of various thicknesses during strain loading. (b) Size dependence of Young's modulus of thin films.

in either case. Dai *et al.*[26] showed that the mechanical properties of ZnO nanowires (Young's modulus and UTS) are size-independent, as long as the nanowires are large enough to sustain a completely crystalline configuration. Our results show that the movement of surface layer atoms affects only Young's modulus. At this stage, we want to highlight the similarities as well as the differences in the mechanical properties of the ZnS nanowires with those of the ZnO nanowires, as has been reported earlier by Kulkarni *et al.*[25] using classical MD simulation with similar kinds of interaction potential. They reported a wurtzite-ZnO to graphitic-ZnO structural transformation in the [01$\bar{1}$0] nanowires and no structural transformation in the [0001] nanowires under stretching. In contrast, for the ZnS nanowires studied here, we do not observe any phase transformation in either direction. It was also reported that both Young's modulus and the UTS values have strong size dependence along the [0001] and [01$\bar{1}$0] directions of ZnO nanowires. In contrast, for ZnS nanowires, we do not find strong size dependence of Young's modulus in the [01$\bar{1}$0]direction. Also, UTS values in neither direction exhibit sharp size dependence.

To verify the reversibility of tensile responses, we calculate the stress-strain relation during the unloading of the nanowire (Figure 11) at the same strain rate as that of loading. The unloading process starts near the top point of the elastic region. As shown in Figure 11(b), strains up to $\sim$13% can be recovered, highlighting a very unusual behavior of ZnS nanowires. Similar high-strain elastic response is also seen in ZnO nanowires.[41] The stress-strain response during loading and unloading processes shows that there is not much hysteresis, so the associated energy dissipation will be very small, which makes these nanowires better suited for building devices in which frequent loading-unloading at high strain is needed.

To understand the effect of dimensionality on the mechanical properties, we also investigate the elastic stiffness of thin films, as shown in Figure 1(e). Because of the larger number of particles, we consider films of smaller thickness only compared with the diameter of the nanowires. The tensile load is applied along the [0001] direction. To simulate the mechanical properties of thin films, we take the length of the simulation box to be the same as the size of the film in the two lateral directions, and in the transverse direction, the simulation box length is taken to be considerably larger than the thickness of the film. Periodic boundary conditions cause the thin film to extend effectively to infinity in two lateral directions, and in the third direction, the interaction between the film and its images is negligible. Strain-stress relationships for thin films are shown in Figure 12(a). From the stress-strain relationship, we calculate Young's modulus. The values of Young's modulus for various film thicknesses are given in Table III. Figure 12(b) shows that the size dependence of Young's modulus is qualitatively similar to that of [0001] nanowires (i.e., Young's moduli of thin films increase as their thickness decreases). More specifically, Young's modulus increases by as much as 41%, 23%, 9%, and 4% for thin films of thickness 0.8, 1.5, 2.3, and 3.0 nm, respectively, compared with bulk ZnS. In Figure 13(a), we compare the size dependence of Young's modulus values of cylindrical nanowires with that of thin films, and we see that Young's modulus of thin films converges more rapidly to the bulk value than that of the nanowires. A film under uniaxial tension can be thought as a row of many wires placed side-by-side under identical axial tension, as shown in Figure 13(b). However, the surface area of the thin film is much smaller than that of the row of nanowires, which might explain the faster convergence of Young's modulus of thin films to its bulk value.

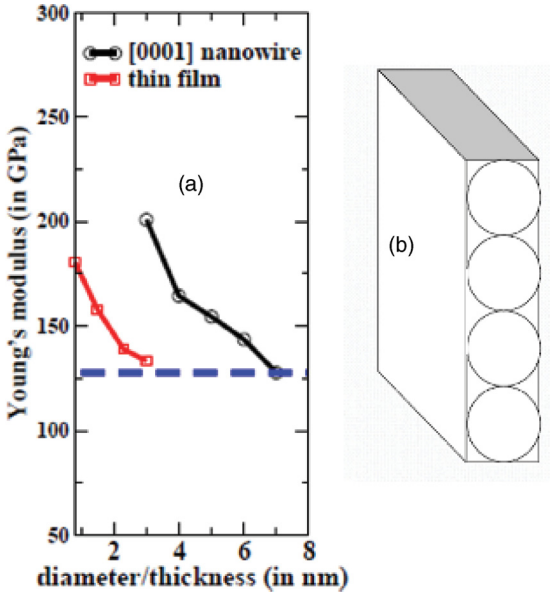

FIG. 13. (Color online) (a) Comparison of Young's modulus values of cylindrical nanowires with those of thin films. (b) Schematic diagram of a thin film, which can be thought of as an array of nanowires placed side by side under the same uniaxial strain. However, for the thin film, the surface to volume ratio will be lower than that of nanowires.

IV. CONCLUSION

In summary, the mechanical behavior of ZnS at the nanoscale is studied using MD simulations for two different growth directions. Young's moduli and UTS of nanowires and thin films are calculated. Nanowires of different growth directions show different behavior under loading. There is a clear size dependence of Young's modulus of [0001] nanowires. On the other hand, Young's modulus of [01$\bar{1}$0] nanowires does not show much size dependence in the particular size range we have investigated. The physical origin of the size dependence of Young's modulus can be attributed to the induced surface stresses due to a high surface to volume ratio at the nanoscale. We provide a microscopic picture of this dependence on size and growth direction. Our study shows that there are both expansion and contraction of bond lengths in a few surface layers. Overall, there is a net contraction of the bond length in [0001] nanowires, and this gives rise to surface stresses responsible for the size dependence of Young's modulus. In contrast, in the [01$\bar{1}$0] direction there are no well-defined surface and core regions. The structural rearrangements occur throughout the sample, making this direction unfavorable for growth. The mean bond length is the same as that in the bulk and surface stresses that lead to a strong size dependence of Young's modulus are not present. To understand the mechanical behavior of ZnS in two dimensions, we calculate the Young's modulus of thin films, which converges to the bulk value more rapidly than that of nanowires under tensile strain in the same direction. This is because of lower surface to volume ratio in thin films. We also calculate the ultimate tensile stresses of nanowires and thin films, which do not have much size dependence. Breaking of nanowires and thin films shows that they are very brittle in nature. We would also like to highlight that in our calculations we have not considered the effects of solvent or surface passivation by capping agents normally used in experiments. These may play an important role in governing the mechanical as well as electronic properties of the nanowires and thin films.

ACKNOWLEDGMENTS

We thank the Department of Science and Technology (DST), India, and MONAMI (Indo-EU project) for financial support. T.M. thanks Council of Scientific and Industrial Research (CSIR), India, for a fellowship.

*taraknath@physics.iisc.ernet.in
†maiti@physics.iisc.ernet.in
‡cdgupta@physics.iisc.ernet.in

[1] T. V. Prevenslik, J. Lumin. **87-9**, 1210 (2000).
[2] C. Falcony, M. Garcia, A. Ortiz, and J. C. Alonso, J. Appl. Phys. **72**, 1525 (1992).
[3] Q. Li and C. R. Wang, Appl. Phys. Lett. **83**, 359 (2003).
[4] Y. C. Zhu, Y. Bando, and D. F. Xue, Appl. Phys. Lett. **82**, 1769 (2003).
[5] B. Y. Geng, L. D. Zhang, G. Z. Wang, T. Xie, Y. G. Zhang, and G. W. Meng, Appl. Phys. Lett. **84**, 2157 (2004).
[6] Y. Jiang, X. M. Meng, J. Liu, Z. R. Hong, C. S. Lee, and S. T. Lee, Adv. Mater. **15**, 1195 (2003).
[7] C. Ma, D. Moore, J. Li, and Z. L. Wang, Adv. Mater. **15**, 228 (2003).
[8] Y. Jiang, X. M. Meng, J. Liu, Z. Y. Xie, C. S. Lee, and S. T. Lee, Adv. Mater. **15**, 323 (2003).
[9] Y. C. Zhu, Y. Bando, D. F. Xue, and D. Golberg, Adv. Mater. **16**, 831 (2004).
[10] Q. Li and C. R. Wang, Appl. Phys. Lett. **82**, 1398 (2003).
[11] Q. H. Xiong, G. Chen, J. D. Acord, X. Liu, J. J. Zengel, H. R. Gutierrez, J. M. Redwing, L. Voon, B. Lassen, and P. C. Eklund, Nano Lett. **4**, 1663 (2004).
[12] Y. W. Wang, L. D. Zhang, C. H. Liang, G. Z. Wang, and X. S. Peng, Chem. Phys. Lett. **357**, 314 (2002).
[13] B. Y. Geng, X. W. Liu, Q. B. Du, X. W. Wei, and L. D. Zhang, Appl. Phys. Lett. **88**, 163104 (2006).
[14] X. M. Meng, J. Liu, Y. Jiang, W. W. Chen, C. S. Lee, I. Bello, and S. T. Lee, Chem. Phys. Lett. **382**, 434 (2003).
[15] X. J. Xu, G. T. Fei, W. H. Yu, X. W. Wang, L. Chen, and L. D. Zhang, Nanotechnology **17**, 426 (2006).
[16] H. Zhang, S. Y. Zhang, S. Pan, G. P. Li, and J. G. Hou, Nanotechnology **15**, 945 (2004).
[17] C. H. Ye, X. S. Fang, G. H. Li, and L. D. Zhang, Appl. Phys. Lett. **85**, 3035 (2004).
[18] S. H. Yu and M. Yoshimura, Adv. Mater. **14**, 296 (2002).

[19]B. Y. Geng, X. W. Liu, J. Z. Ma, Q. B. Du, and L. D. Zhang, Appl. Phys. Lett. **90**, 183106 (2007).
[20]Y. C. Zhu, Y. Bando, and Y. Uemura, Chem. Commun. 836 (2003).
[21]B. Elidrissi, M. Addou, M. Regragui, A. Bougrine, A. Kachouane, and J. C. Bernede, Mater. Chem. Phys. **68**, 175 (2001).
[22]H. Ni and X. D. Li, Nanotechnology **17**, 3591 (2006).
[23]R. Agrawal, B. Peng, E. E. Gdoutos, and H. D. Espinosa, Nano Lett. **8**, 3668 (2008).
[24]M. Lucas, W. J. Mai, R. S. Yang, Z. L. Wang, and E. Riedo, Nano Lett. **7**, 1314 (2007).
[25]A. J. Kulkarni, M. Zhou, and F. J. Ke, Nanotechnology **16**, 2749 (2005).
[26]L. Dai, W. C. D. Cheong, C. H. Sow, C. T. Lim, and V. B. C. Tan, Langmuir **26**, 1165 (2010).
[27]R. Agrawal, J. T. Paci, and H. D. Espinosa, Nano Lett. **10**, 3432 (2010).
[28]X. D. Li, X. N. Wang, Q. H. Xiong, and P. C. Eklund, Nano Lett. **5**, 1982 (2005).
[29]Q. H. Xiong, N. Duarte, S. Tadigadapa, and P. C. Eklund, Nano Lett. **6**, 1904 (2006).
[30]C. Q. Chen, Y. Shi, Y. S. Zhang, J. Zhu, and Y. J. Yan, Phys. Rev. Lett. **96**, 075505 (2006).
[31]H. X. Chen, D. N. Shi, J. S. Qi, and B. L. Wang, Physica E: Low-Dimensional Systems and Nanostructures **42**, 32 (2009).
[32]R. E. Miller and V. B. Shenoy, Nanotechnology **11**, 139 (2000).
[33]V. B. Shenoy, Phys. Rev. B **71**, 094104 (2005).
[34]A graphical molecular modelling program developed by Accelrys Inc.
[35]See Supplemental Material at http://link.aps.org/supplemental/10.1103/PhysRevB.86.024101 for the convention used to determine the sizes of nanowires and thin films.
[36]K. Wright and R. A. Jackson, J. Mater. Chem. **5**, 2037 (1995).
[37]J. P. Perdew, K. Burke, and M. Ernzerhof, Phys. Rev. Lett. **77**, 3865 (1996).
[38]P. Giannozzi, S. Baroni, N. Bonini, M. Calandra, R. Car, C. Cavazzoni, D. Ceresoli, G. L. Chiarotti, M. Cococcioni, I. Dabo, A. Dal Corso, S. de Gironcoli, S. Fabris, G. Fratesi, R. Gebauer, U. Gerstmann, C. Gougoussis, A. Kokalj, M. Lazzeri, L. Martin-Samos, N. Marzari, F. Mauri, R. Mazzarello, S. Paolini, A. Pasquarello, L. Paulatto, C. Sbraccia, S. Scandolo, G. Sclauzero, A. P. Seitsonen, A. Smogunov, P. Umari, and R. M. Wentzcovitch, J. Phys.: Condens. Matter **21**, 395502 (2009).
[39]H. J. Monkhorst and J. D. Pack, Phys. Rev. B **13**, 5188 (1976).
[40]V. K. Sutrakar and D. R. Mahapatra, J. Phys.: Condens. Matter **20**, 335206 (2008).
[41]A. J. Kulkarni, M. Zhou, K. Sarasamak, and S. Limpijumnong, Phys. Rev. Lett. **97**, 105502 (2006).
[42]C. F. Cline, H. L. Dunegan, and G. W. Henderso, J. Appl. Phys. **38**, 1944 (1967).
[43]S. H. Na and C. H. Park, J. Korean Phys. Soc. **56**, 498 (2010).
[44]D. Moore and Z. L. Wang, J. Mater. Chem. **16**, 3898 (2006).
[45]J. Zhang, Y. D. Yang, F. H. Jiang, J. P. Li, B. L. Xu, X. C. Wang, and S. M. Wang, Nanotechnology **17**, 2695 (2006).
[46]Y. N. Xu and W. Y. Ching, Phys. Rev. B **48**, 4335 (1993).
[47]R. R. Reeber and G. W. Powell, J. Appl. Phys. **38**, 1531 (1967).
[48]C. E. Hu, L. L. Sun, Z. Y. Zeng, and X. R. Chen, Chin. Phys. Lett. **25**, 675 (2008).
[49]C. Y. Yeh, Z. W. Lu, S. Froyen, and A. Zunger, Phys. Rev. B **46**, 10086 (1992).
[50]M. Catti, Y. Noel, and R. Dovesi, Journal of Physics and Chemistry of Solids **64**, 2183 (2003).